We are IntechOpen, the world's leading publisher of Open Access books Built by scientists, for scientists

4,800
Open access books available

122,000
International authors and editors

135M
Downloads

Our authors are among the

154
Countries delivered to

TOP 1%
most cited scientists

12.2%
Contributors from top 500 universities

CLARIVATE ANALYTICS BOOK CITATION INDEX INDEXED

WEB OF SCIENCE™

Selection of our books indexed in the Book Citation Index in Web of Science™ Core Collection (BKCI)

Interested in publishing with us?
Contact book.department@intechopen.com

Numbers displayed above are based on latest data collected.
For more information visit www.intechopen.com

2

Evaluation of Uni-Traveling Carrier Photodiode Performance at Low Temperatures and Applications to Superconducting Electronics

Hideo Suzuki
International Superconductivity Technology Center
Japan

1. Introduction

High-speed photodiodes are useful devices for optical-telecommunication systems and scientific applications. A uni-traveling carrier photodiode (UTC-PD), has extremely wide band performance of over 300 GHz and used for many high-frequency or high-speed applications. Signal transmission using optical fibers, which has several advantages such as its wide band transmission and low transmission loss, is an indispensable technology that forms the foundation of the Internet. Optical fibers also exhibit low thermal conductance and are capable of electrical isolation. These features are useful for interfacing between low-temperature and room-temperature electronics. Superconducting devices and circuits are attractive for high-speed, low-power, and quantum mechanical operations.

However, such devices and circuits have to be cooled below the critical temperatures of superconducting materials, Tc. For high-temperature superconducting materials such as YBCO, the operating temperature is around that of liquid nitrogen, 77 K, and for low-temperature metal-based superconducting materials, such as Nb and NbN, the operating temperature is around that of liquid helium, 4 K. Input/output links are one of the bottle necks preventing practical application of superconducting devices and circuits. In particular, devices and circuits using low-temperature superconductors exhibit serious problems because the high-frequency electrical I/O cables consume a large amount of cooling power. However, cooling power, especially at around 4 K and below, is quite small, typically less than 1 W, though the input AC power is as large as several KW. The amount of AC input power can be reduced by reducing the cooling power. Our goal is to use a compact cryocooler. Such a cryocooler has limited cooling capability; however, it is enough for most applications of superconducting devices due to their low power requirements. Optical I/O has potential to overcome the problem by using optical fibers and photo devices such as photodiodes. A UTC-PD seems to be the most attractive device because of its high-speed performance and is required to operate at low temperatures for application in superconducting systems. In this chapter, we describe UTC-PD performance at low temperatures and its applications in superconducting systems.

2. Customized structure and dc characteristics of UTC-PD module at low temperatures

We investigated the performance of a UTC-PD chip and modules at low temperature, which had not been done previously. The response at temperatures as low as 4 K was characterized for a commercially available standard UTC-PD module and a customized one we developed for superconducting devices. To apply the UTC-PD modules into various superconducting analog devices and systems using superconducting microchips (ICs) of digital and analog/digital circuits, the UTC-PD modules should be located near the superconducting ICs to maintain signal integrity. Ferromagnetic materials, which are widely used in many optical components, are used in the standard UTC-PD module. In general, superconducting devices and microchips, such as single flux quantum (SFQ) circuits and Josephson voltage standards (JVS), are strongly affected by the remnant magnetic field. Therefore, these materials must not be used near the chips. Hence, we developed a UTC-PD module using a customized package and a fiber lens technique for superconducting devices.

2.1 Band diagram and gap energy at cryogenic temperature

We studied the characteristics of a UTC-PD chip at low temperatures. The energy band diagram of a UTC-PD chip is illustrated in Fig. 1. The electrons generated by incoming optical irradiation in the InGaAs absorption layer are transported at high-speed to the InP wideband-depleted and n^+InP layers with drift by electrical field. In principle, UTC-PD uses the electrons as minority carriers for transporting current, which determines the operating speed. On the other hand, holes are not important for operating speed because those in the InGaAs layer are majority carriers and respond with dielectric relaxation time. This situation differs from a commonly used pin photo diode (pin-PD) using electrons and holes as minority carriers in the depletion layer. The features of a UTC-PD chip enable it to respond faster than a commonly used pin-PD chip. The optical absorption layer consists of

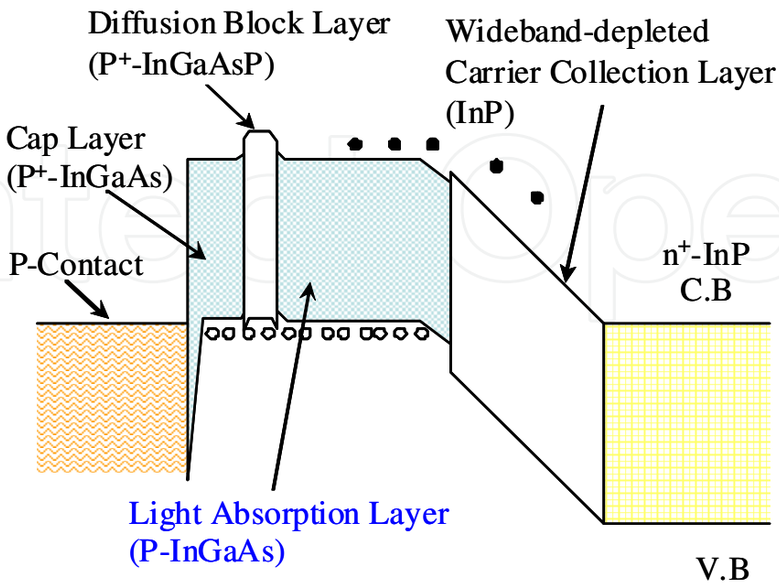

Fig. 1. Band diagram of uni-traveling carrier photodiode (UTC-PD).

$In_{1-x}Ga_xAs$ (x=0.47). The temperature dependence of the absorption coefficient vs. photon energy of the InGaAs can be seen in the handbook series on semiconductor parameters editted by Goldberg Yu.A. and N.M. Schmidt. The photon energy, at which the absorption is decreased, is critical for low-temperature performance. The transition point of the photon energy was plotted based on the handbook, as shown in Fig. 2. The wavelength, $\lambda=hc/E$, and the energy corresponding to the photon energy, E, are also plotted in this figure. Basically, a UTC-PD chip does not seem to have sensitivity at a wavelength of 1550 nm to optical irradiation at cryogenic temperature between 4 – 77 K. However, we assume that they must have sensitivity even at cryogenic temperature because the absorption layer, the InGaAs layer, is p-doped, blurring the band edge of the conduction band.

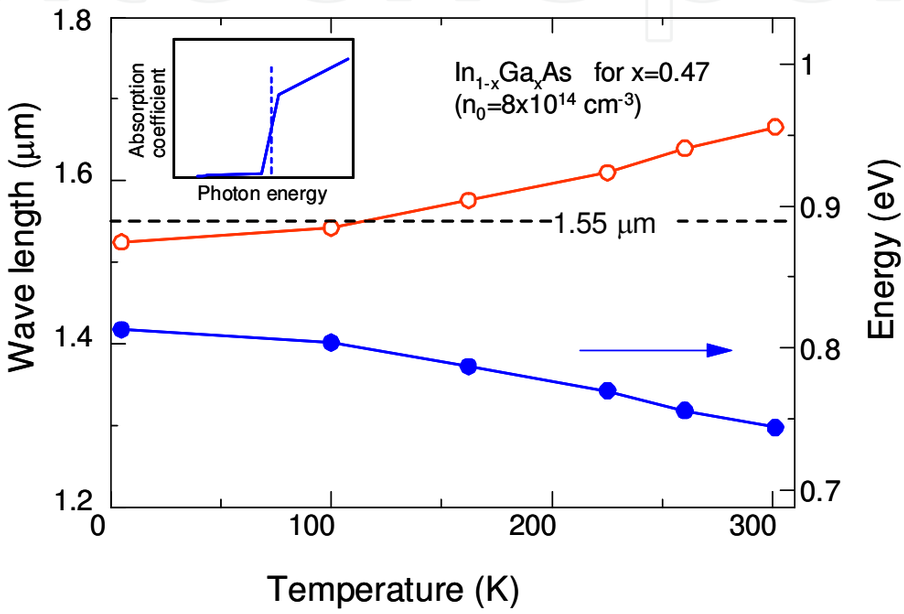

Fig. 2. Gap energy and its corresponding wavelength dependence as function of temperature for $In_{1-x}Ga_xAs$ (x=0.47) used as absorption layer in UTC-PD.

2.2 Structure and optical dc sensitivity at low temperature

Figure 3 shows an illustration of two types of UTC-PD modules, standard and customized. The photo diode chips have the same specifications as follows, over 60-GHz band width, negative type output, optical acceptance area of 100 μm^2, incident light irradiated to the edge of the chip, which is chemically etched along the facet of the InP substrate, and facet angle of 55 degrees, making the incident angle 35 degrees to the facet. Hence, the incident light comes from the InP substrate to the absorption layer. The standard module has two lenses, collimation and focus, between the optical fiber and the UTC-PD chip to effectively introduce the light, as shown in Fig. 3(a). In this structure, ferromagnetic cobalt material is commonly used to fix the lenses in the package. For most applications of superconducting electronics, however, remnant magnetism must be avoided for use near superconducting ICs. Therefore, an optical fiber lens technique, in which the optical fiber is rounded at the edge, is used in the customized UTC-PD module instead of normal optical lenses, as shown in Fig. 3(b). The working distance between the fiber lens and chip is around 80 μm in the customized module.

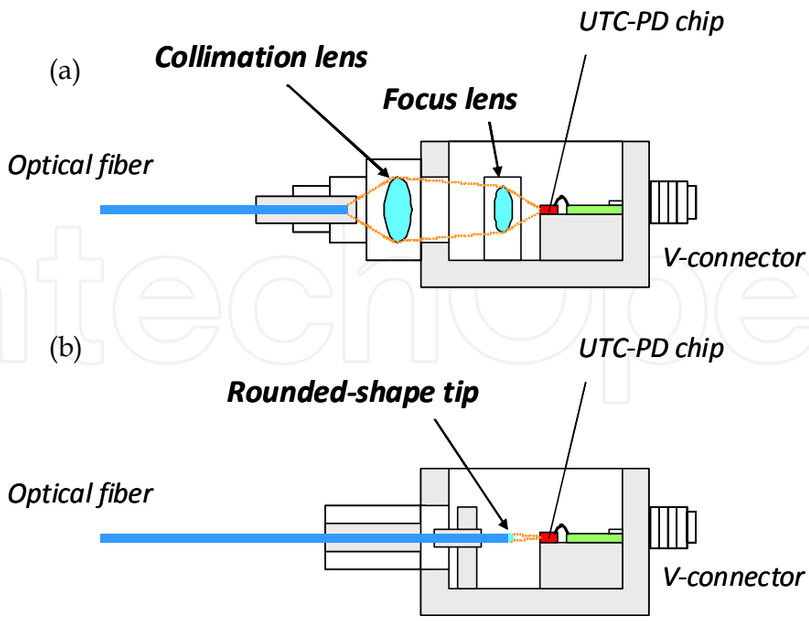

Fig. 3. Structures of (a) standard UTC-PD module, and (b) non-magnetic UTC-PD module using fiber lens specialized for superconducting device.

The beam size is 8 μm in $1/e^2$ reduction of the intensity, and the tolerance of the beam position for optical coupling is shown in Fig.4. Optical output reduction was 50% for a beam position movement of 3 μm from the ideal central position. The optical beam was irradiated from the edge of the UTC-PD chip, which corresponds to an incident angle of 35 degrees to the facet of the InP substrate. One of the important problems with our customized module is that the optical axis is misaligned, when the module is cooled to cryogenic temperature. The optical sensitivity of our customized UTC-PD module at around 4 K was reduced to less than one tenth of that at 300 K in the initial version, which was developed in the beginning

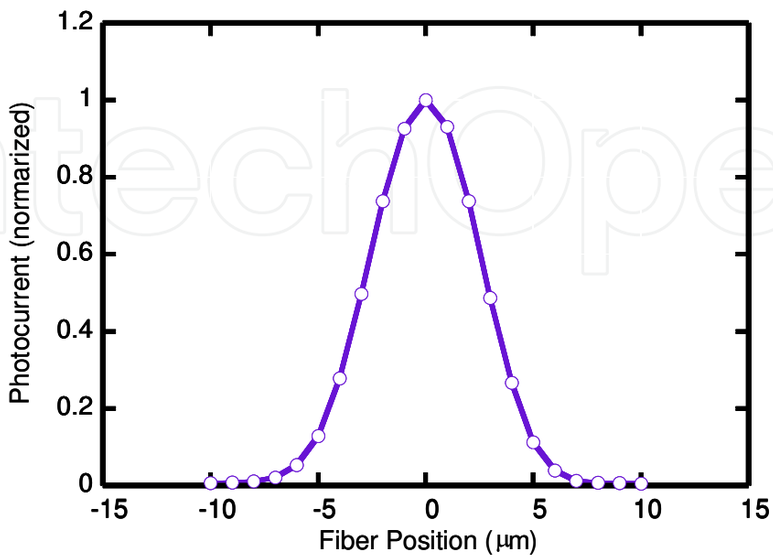

Fig. 4. Intensity dependence of beam on offset distance from ideal central position.

of the customized modules. On the other hand, misalignment did not occur for the standard one. The cause of the misalignment was due to the bending of the optical fiber. The problem was finally resolved by shortening the free space of the fiber without ferrule and by uniformly gluing the fiber to the ferrule with epoxy resin, as shown in Fig. 5(a). Figure 5(b) is a photograph of the entire module, which has a coaxial V-connector for a wide-band electrical output and DC terminals.

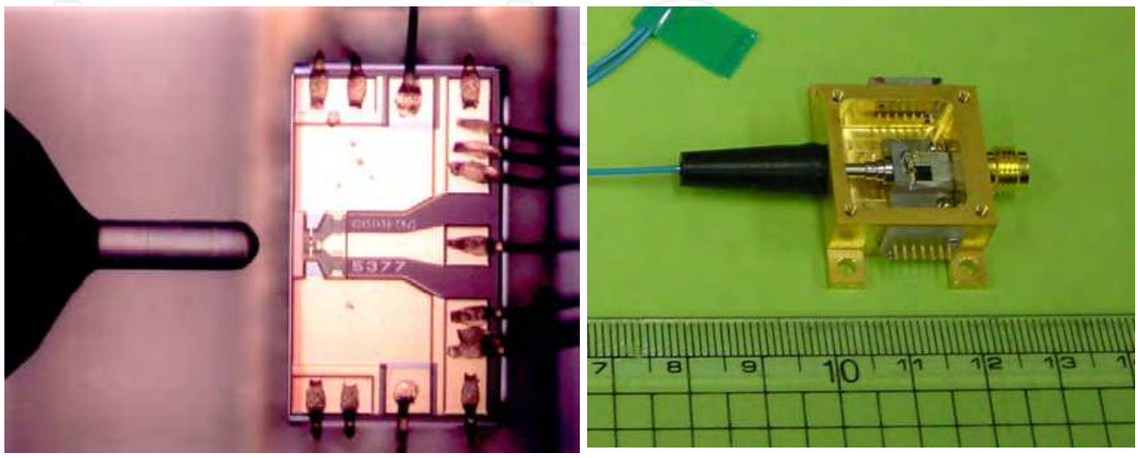

(a) (b)

Fig. 5. Photographs of customized UTC-PD; (a) UTC-PD chip and fiber lens and (b) entire module.

The equivalent circuit of a negative type UTC-PD module is shown in Fig. 6. In the negative type, the UTC-PD module is usually negatively biased to accelerate electron drift in the depletion layer, increasing the operating speed. The output signal is inverted to the input signal. A termination resistor of 50 Ω for impedance matching is integrated at the output of the chip.

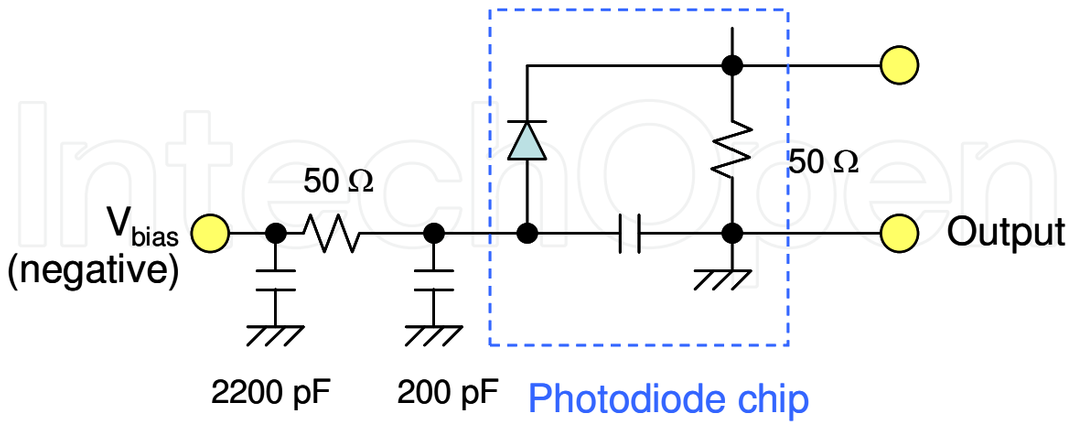

Fig. 6. Equivalent circuit of negative-type UTC-PD module.

2.3 DC characteristics at low temperature

The current versus voltage (I-V) characteristics of our customized UTC-PD module was measured at operating temperatures from 4 to 300 K, as shown in Fig. 7. No electrical and

mechanical damage was observed from the I-V characteristics in our experiments when the UTC-PD module was cooled using a cryocooler at a cooling rate of around 1 degree/minute. Since the gap energy of the InGaAs increased and thermal energy decreased, the forward voltage, at which the current rapidly increased, somewhat increased. The forward voltage increased around 0.16 V by cooling from 300 K to 4 K. The forward current increased sharply at this forward voltage as the operating temperature decreased.

Dependence of optical sensitivity on temperature was measured for both modules, as shown in Fig. 8. The optical wave length was 1550 nm and the input optical power was 0.7 W. Both the UTC-PD modules were biased at -2 V, and the output voltage was measured with a digital voltmeter. The output voltage decreased as the temperature decreased. The output voltage of the standard UTC-PD module was larger than that of customized UTC-PD module over the entire temperature range. The temperature dependences, however, showed relatively similar changes between the two modules. The difference in the results for the two modules was probably due to the difference in the coupling efficiency between the lens and the chip. The output voltage of the customized module is still large enough. We can, therefore, conclude that the customized module using a fiber lens is useful for most applications that require a non-magnetic environment, such as those for superconducting devices.

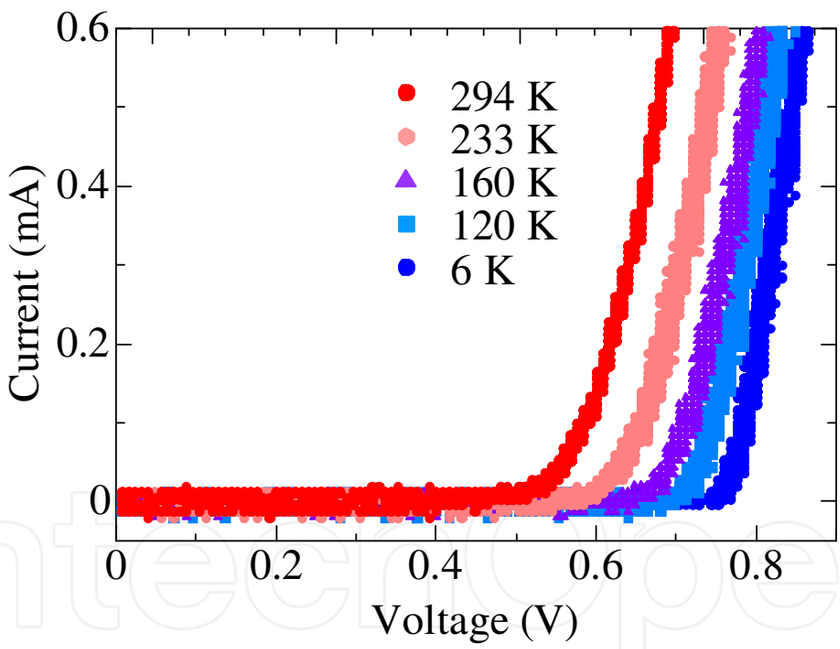

Fig. 7. Current versus voltage (I-V) curves at temperatures between 6 and 294 K.

3. High-frequency and high-speed operation

The high-frequency response of a UTC-PD module at low temperature is important. We evaluated this response using a high-speed optical measurement system. We needed several electronic and optical instruments to produce an optical signal modulated with various high-speed bit pattern signals. The measurement system and the high-speed response of our customized UTC-PD module are discussed in this section. The cryocooling system for cooling the customized UTC-PD module and superconducting devices is discussed in the next section.

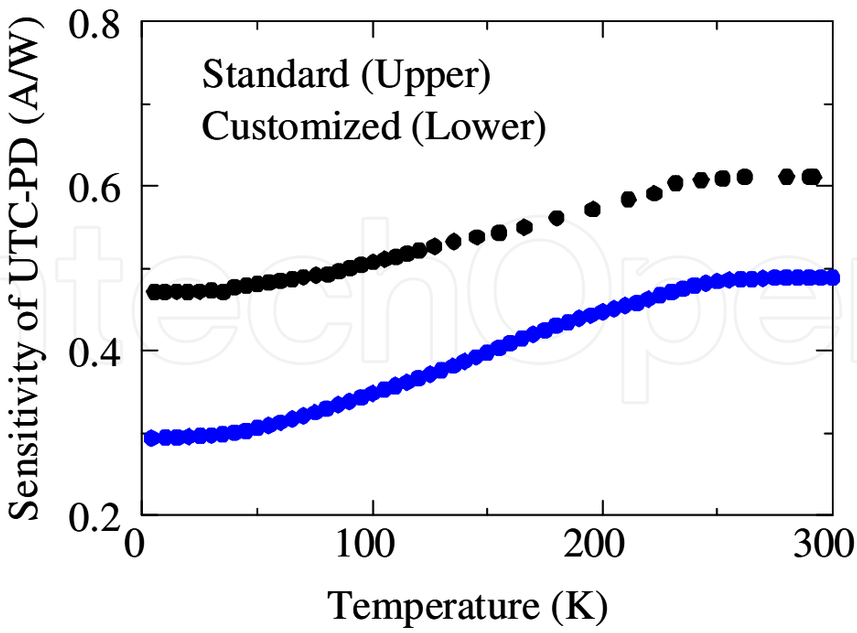

Fig. 8. Temperature dependence of sensitivity of standard and customized UTC-PD modules.

3.1 Optical input measurement system

Figure 9 shows a block diagram of the optical measurement system, which can output 47-Gbps high-speed optical signals. The main clock signal is generated with a signal generator (Anritsu MG3695B: 2 - 50 GHz), and the pulse pattern is generated with a 4-channel pulse pattern generator (Anritsu MP1758A: 10 MHz - 12.5GHz) and serialized with a multiplexer (MUX), which enables us to generate a non-return-to-zero (NRZ) pulse pattern of up to 47 GHz. The MUX and pulse pattern generator (PPG) were synchronized and the timing of the digital data from the PPG to the clock signal in the MUX was adjusted with delay lines. An electrical/optical (E/O) converter with a MUX (Anritsu MP1806A), which includes a laser diode, an optical modulator with an automatic bias controller (ABC), generated arbitrary optical digital pattern signals with a modulation depth of almost 100%. The optical signal was amplified with an erbium-doped fiber amplifier (EDFA) and the output power was adjusted with a power controller and attenuator (Agilent 8163B). The controlled output signal was applied to the customized UTC-PD module, which converted the optical signal to an electrical signal at around 4 K. The electrical output was connected to a cryoprobe, which was also cooled at around 4 K, through a 1.19-mmϕ copper coaxial cable of 230 mm in length.

3.2 High-frequency performance

The high-speed performance of the customized UTC-PD module cooled around 4 K was measured and confirmed for up to a 40-Gbps NRZ signal. The customized UTC-PD module was set on the 2nd stage in the cryocooling system, which is discussed in Section 4.1. Figures 10(a) and (b) show typical eye diagrams of the input optical signal and the output electrical signal observed with a sampling oscilloscope (Agilent 86100C). The modulation depth was automatically adjusted to almost 100%. The input signal was a pseudo random bit stream (PRBS) signal with a data length of 2^{31}-1. A block diagram of the measurement system is

shown in Fig. 9. The output line includes a loss of 2.8 dB at 40 GHz in a 510-mm-long coaxial cable in the cooling system.

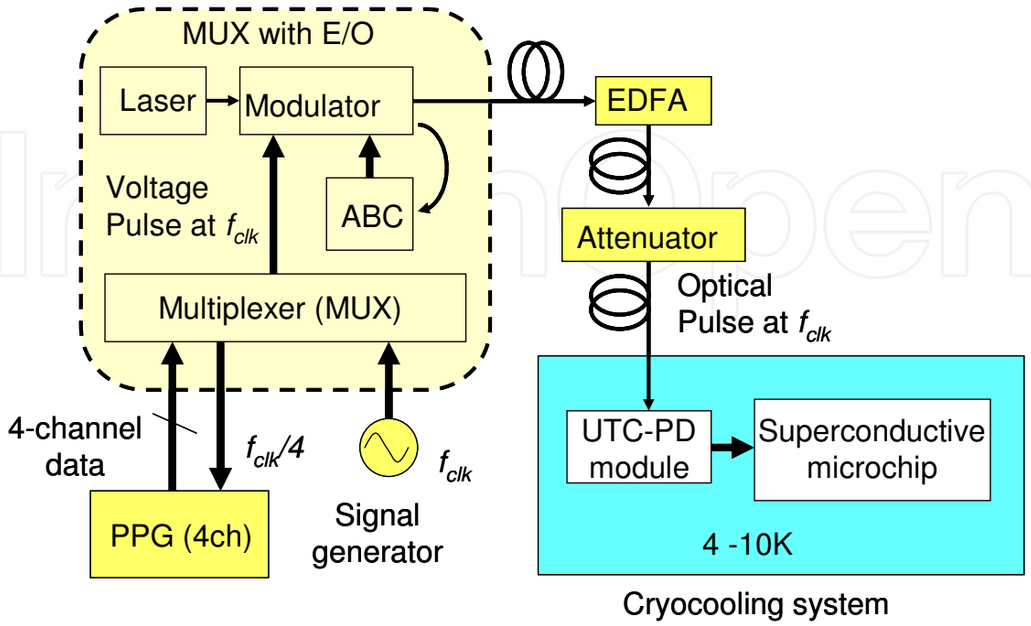

Fig. 9. Setup of optical measurement system that can produce optical digital signal at data rate of up to 47 Gbps

The amplitude of the output signal was 90 mV in a peak-to-peak voltage for an input optical signal power of 10 mW at a wavelength of 1550 nm. We evaluated the linearity for the amplitude of the output voltage to the optical input signal power. Since there was no difference observed for the data length between 2^{31}-1 and 2^{7}-1 of the PRBS signals, a data length of 2^{7}-1 was used to save time. Figure 11 shows the optical input power versus the output voltage for 10, 20, and 40-Gbps PRBS data input, resulting in good linearity over the input optical power of 10 mW. In the above evaluation, the customized UTC-PD module

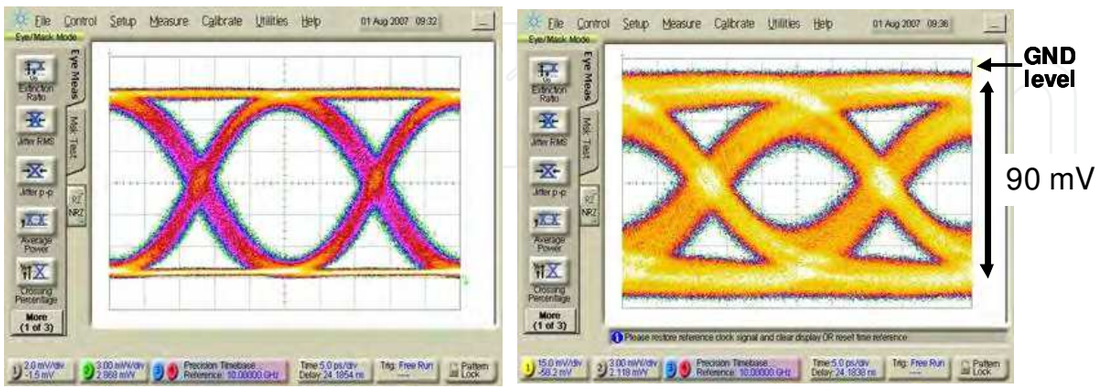

(a) (b)

Fig. 10. Eye patterns of (a) optical output signal of optical measurement system for 31-stage pseudo random bit stream (PRBS) digital signal and (b) electrical output signal of customized UTC-PD module cooled at 5 K.

was DC biased at -2 V, which is definitely required for high-speed performance at room temperature. It should be noted that the customized UTC-PD module operated at high speed even at zero DC bias voltage, which may be due to the increment of the built-in electric field in the absorption and depletion layers.

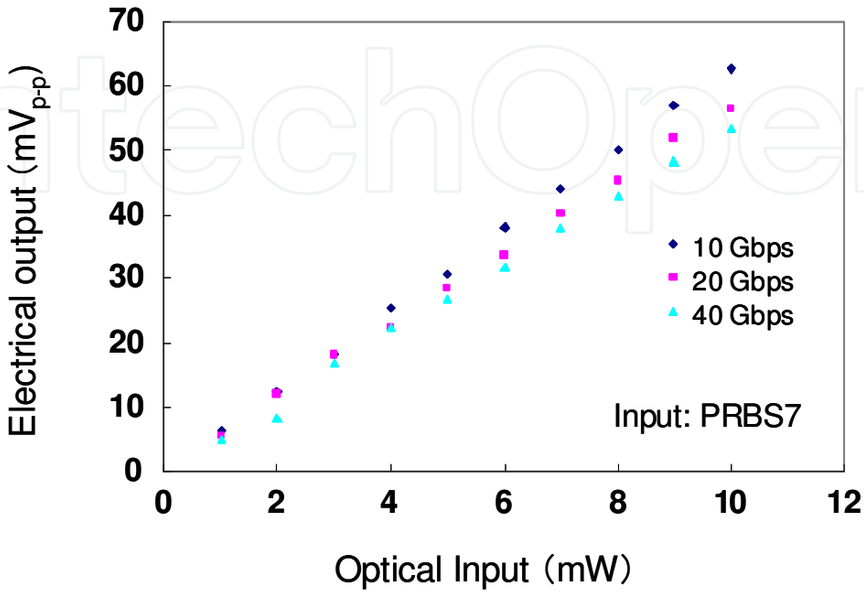

Fig. 11. Electrical output voltages as function of optical input power of customized UTC-PD module cooled at 5 K for 10, 20, and 40-Gbps PRBS data input.

4. Applications of UTC-PD module operating at cryogenic temperature to superconducting electronics

The optical link of the input signal between semiconducting devices operating at room temperature and superconducting devices at cryogenic temperature has several advantages. The thermal conductivity of optical fibers is extreamly small compared with metal-based electric links, such as coaxial and flexible film cables. The themal conductivity of quatz, which is a base material in a single-mode opitical fiber, is 1.4 W/m/K; therefore, the thermal conductivity of a single-mode optical fiber having a crad diameter of 125 μm and a length of 1 m is as small as 5.2×10^{-6} W. The signal loss is also extremely small, e.g., < 0.2 dB/km for a wavelength of 1550 nm and < 0.4 dB/km for 1310 nm. The signal loss of the optical fiber is negligible for our applications such as analogue to digital converters (ADC) using SFQ circuits, which require short distance transmission. It is small enough even if we use a longer, e.g., 1 km, optical fiber. The signal loss seems to be rather large at optical connectors and other parts.

4.1 Cryocooling system for superconducting electronics system

Single flux quantum circuits have been investigated for superconducting digital and analog/digital applications. In most of these investigations, superconducting IC chips were cooled by directly immersing them in liquid helium. It is convenient to cool IC chips to cryogenic temperature for laboratory use due to the immediate cooling time. Many

superconducting systems, however, require a cryocooler for practical applications. Even for laboratory use, a cooling system using a cryocooler is desirable for system-level tests and high-speed or high-frequency tests because the signal loss and distortion between room temperature and cryogenic temperature may especially cause problems and restrict experiments. A cryocooling system using a two-stage 4-K Gifford MacMahon (GM) cryocooler was developed at the international Superconductivity Technology Center (ISTEC) for demonstrating superconducting digital and analog ICs based on the Nb/AlOx/Nb Josephson junctions. A photograph and illustration of the system is shown in Fig. 12. The 2nd cold stage, 4-K stage, including a superconducting chip, a cryoprobe, and our customized UTC-PD module is surrounded with a thermal shield with a temperature of 50 K using the 1st cold stage of the cooler. Cryogenic amplifiers are attached to the thermal shied. The cryocooler (RDK-408D) and the compressor (CSA-71A) are from Sumitomo heavy industries Ltd. The cooling capacity is 1 W at 4.2 K for the 2nd cold stage and 60 W at 50 K for the 1st cold stage. The total input AC power of the cooler is 6.5 kW. The system has twenty-four high-frequency I/O terminals with V-connectors and two optical input ports using the customized UTC-PD module. The 1st cold stage of the cooler, the 50-K stage, can effectively be used for cooling the cryogenic amplifiers, thermal shied, and thermal anchor.

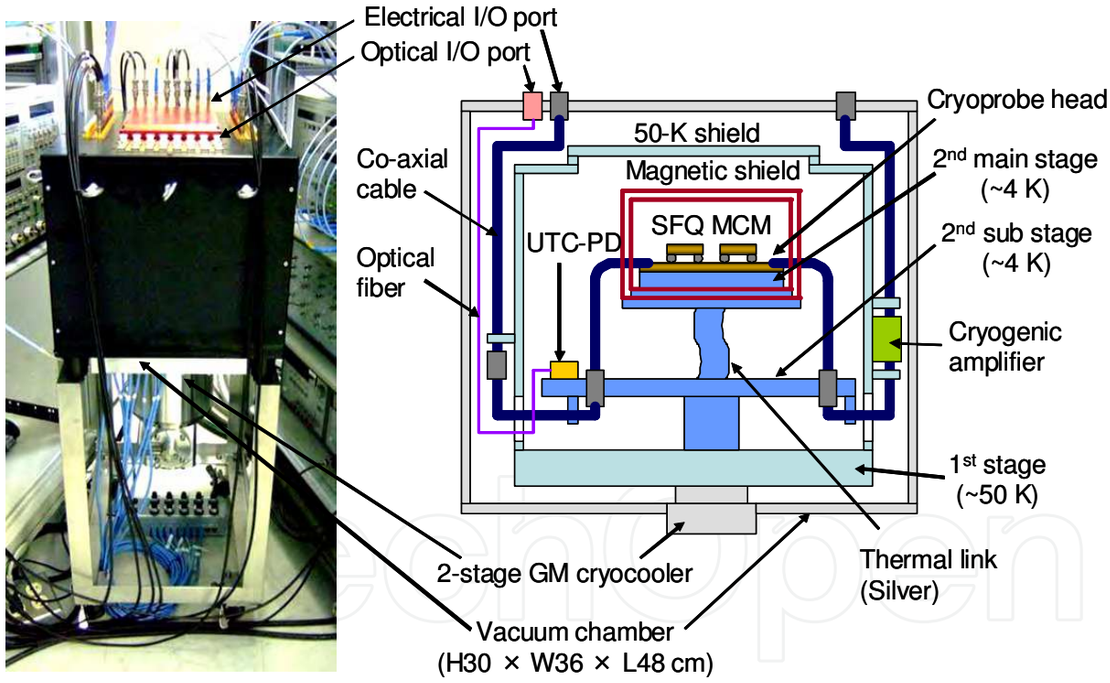

Fig. 12. Cryocooling system for supeconducting devices. Left is photograph of system and right is cross-sectional illustration.

Figure 13 shows a photograph of the 2nd stage arrangement with a cryoprobe and two customized UTC-PD modules placed on the sub 2nd cold stage located in a short distance around 100 mm from the SFQ multi-chip module (MCM) on the main 2nd stage, as shown in Figs. 12 and 13; therefore, the temperature was a little high, between 5-6 K. We developed MCM technology with flip-chip bonding and a cryoprobe for superconducting systems, which enable us to conduct high-speed measurements of superconducting circuits. The SFQ

chips mounted on the MCM substrate including the cryoprobe was attached to the main 2nd stage, which was magnetically shielded with a two-folded permalloy enclosure. However, the customized UTC-PD module was placed outside the magnetic shield. The main 4-K stage was cooled with thermal conduction through a thermal link made of silver and the magnetic shield from the 2nd cold head of the cryocooler. The vibration of the temperature at the main 4-K stage was then stabilized to as low as 10 mK, which ensured the stable operation of SFQ circuits.

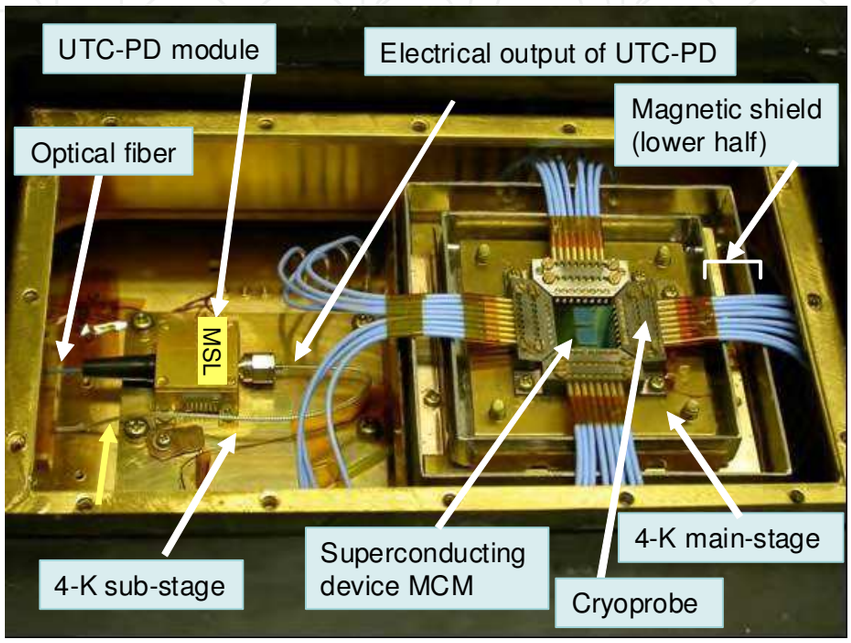

Fig. 13. Arrangement of 4-K cold stages in cooling system; superconducting IC chip with multi-chip module (MCM) and cryoprobe surrounded by double magnetic shield (right side; the lids are removed to show the contents) on main cold stage, and customized UTC-PD module operating at 4 K for introducing high-frequency optical signal into cryostat through optical fiber was placed on sub-cold stage.

4.2 Superconducting single flux quantum (SFQ) digital circuits

We designed an SFQ circuit chip, which includes an input interface between the customized UTC-PD module and SFQ circuit. Figures 14 (a) and (b) show an equivalent circuit and a microphotograph of the PD/SFQ converter. The chip was fabricated with the ISTEC standard process 3 (STP3) using Nb/AlOx/Nb Josephson junctions with a current density of 10 kA/cm^2. The input signal was magnetically coupled to the SFQ circuit, making it possible to accept both polarities of the input signal by changing the direction of the coupling in the transformer. The negative polarity signal from the customized UTC-PD module was then able to be received directly without any offset current and inverter by the PD/SFQ converter shown in Fig. 14. Josephson junctions, J1 and J2, and inductances, L1 and L2, construct a superconducting quantum interference device (SQUID). When the input signal, data "1", is applied, the SQUID stores the single flux quantum in the superconducting loop, producing clockwise circulating current. By applying the clock pulse, the SFQ pulse is output by switching J2 and J3. When data "0" is applied, no SFQ pulse is output. In this case, the SFQ

pulse produced by the clock pulse is escaped from J5. The converter can then produce SFQ pulses from the normal NRZ signal from the customized UTC-PD module, where the SFQ pulse

$$\int V(t)dt = \Phi_0 = h / 2e \sim 2.07 \times 10^{-15}[Wb] \quad (1)$$

acts as the quantized information medium in SFQ circuits.

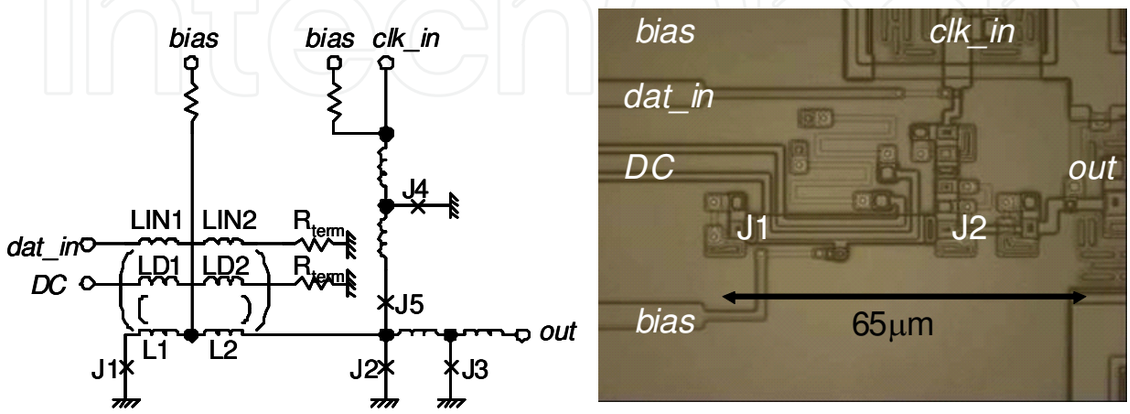

(a) (b)

Fig. 14. UTC-PD to single flux quantum (SFQ) converter; (a) equivalent circuit and (b) microphotograph.

The SFQ circuit chip for testing the optical input link is composed of the PD/SFQ convertor, a 1-2 demultiplexer (DEMUX), and two NRZ superconducting voltage drivers (SVDs), as shown in Fig. 15. Signal flux quantum pulses have a narrow width (~2 ps) and a low signal level (~1 mV), and the circuit can be operated faster than that in semiconductor devices. The SFQ output data of the PD/SFQ is alternately output to the two outputs with the 1:2 DEMUX in parallel to reduce the output data rate to half the input data rate. Then, the SFQ pulse signal is converted to an NRZ signal by the SVDs.

Figure 16 shows an NRZ SQUID voltage driver (NRZ SVD). This NRZ SVD consists of a splitter (SPL), which divides a single SFQ signal into 16 splitter outputs, RS flip-flops (RSFFs), each of which stores an SFQ signal, and 16 serially connected SQUIDs, which amplify the SFQ signal stored in the RSFF to 2-mV NRZ data streams up to 23.5 GHz. There are a total of 318 junctions, and the bias current is 43 mA. The 5 x 5 mm SFQ chip was flip-chip bonded on a 16 mm x 16 mm MCM carrier with InSn bumps, as shown in Fig. 17(a).

Both the chip and carrier are made of the same Si substrate, which prevents stress due to the difference in thermal expansion coefficients when they are cooled. Figure 17 (b) shows InSn bumps for the signal and ground, in which the signal bump was connected to a 50 Ω micro-strip line (MSL) in the chip. The height of the bump was as small as 8 μm, as shown in Fig. 17(c), which enabled us to transmit high-frequency signals over 100 GHz. The MCM carrier was mounted on the 4-K main base plate of the cryoprobe, as shown in Fig. 13. Copper-molybdenum alloy was chosen as the base plate material to decrease the difference in the thermal expansion coefficient. The cryoprobe was adjusted to ensure contact of the chip pads. The optical link was tested using the test circuit at a high-speed data rate.

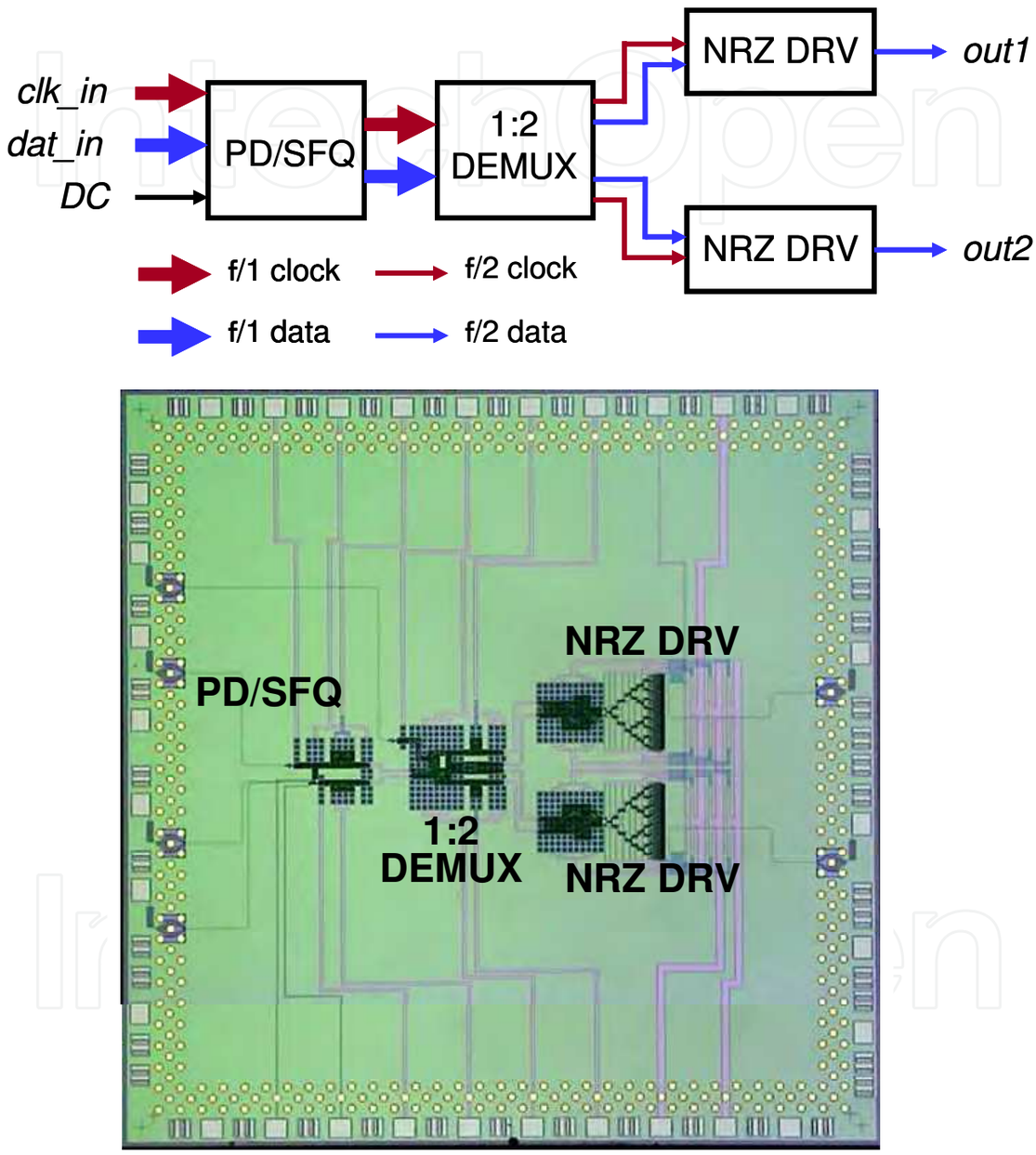

Fig. 15. Block diagram and microphotograph of SFQ test chip for optical input.

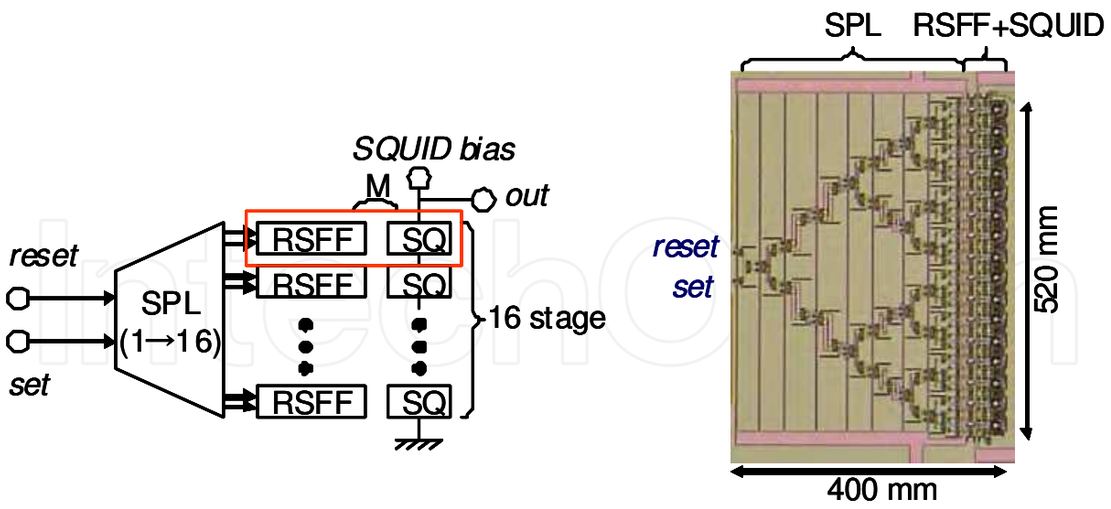

(a) (b)

Fig. 16. Non-return-to-zero (NRZ) superconducting quantum interference device (SQUID) voltage driver; (a) block diagram and (b) microphotograph.

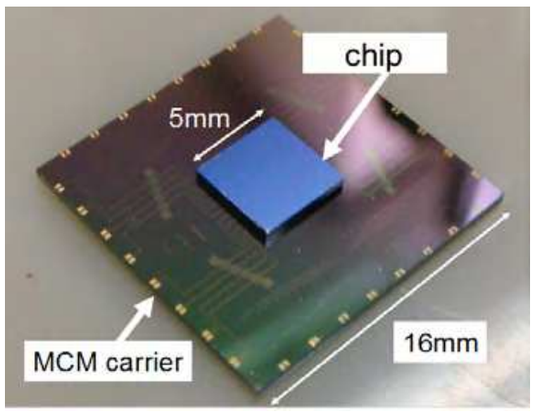

(a)

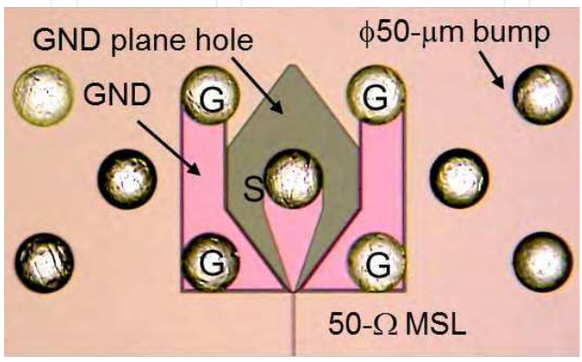

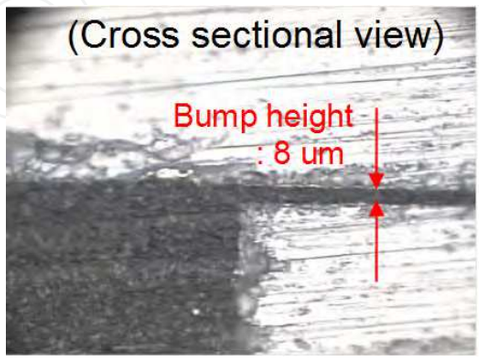

(b) (c)

Fig. 17. Photographs of, (a) flip-chip bonded MCM carrier and superconducting micro-chip, (b) flip-chip bumps on chip, and (c) cross sectional view of flip-chip bonded bump.

The output signals of the SVDs are further amplified by GaAs cryogenic amplifiers mounted on the 1st stage of the cryocooling system, as shown in Fig. 12. The cryogenic amplifier, SHF105C, was developed by SHF communication Technology AG originally for SFQ circuits in collaboration with ISTEC. The output voltage of the SVDs was amplified to around 50 mV with the cryogenic amplifiers, which have a gain of around 30 dB at 23 K and a typical bandwidth of 30 GHz. The optical digital data of up to 47 Gbps was applied to the customized UTC-PD module, and the converted electrical signal was applied to the test chip through a Cu coaxial flexible cable of 1.19 mm in diameter and length of 230 mm. Figure 18 shows the experimental results for the input data rate of 47-Gbps data; (a) the outputs of the two SVDs for patterned digital data and (b) eye pattern for PRBS of 2^{31} -1. We can clearly see an open eye pattern. The bit error rate (BER) was measured with an error detector (Advantest D3286). Figure 19 shows the dependences of the BER for PRBS of 2^{7}-1, (a) on the bias current of the PD/SFQ converter and (b) on the input optical power. Sufficiently small BER of less than 10^{-12} at 40 Gbit/s in the output was obtained with the test circuit for the optical input signal through the customized UTC-PD module as an O/E converter.

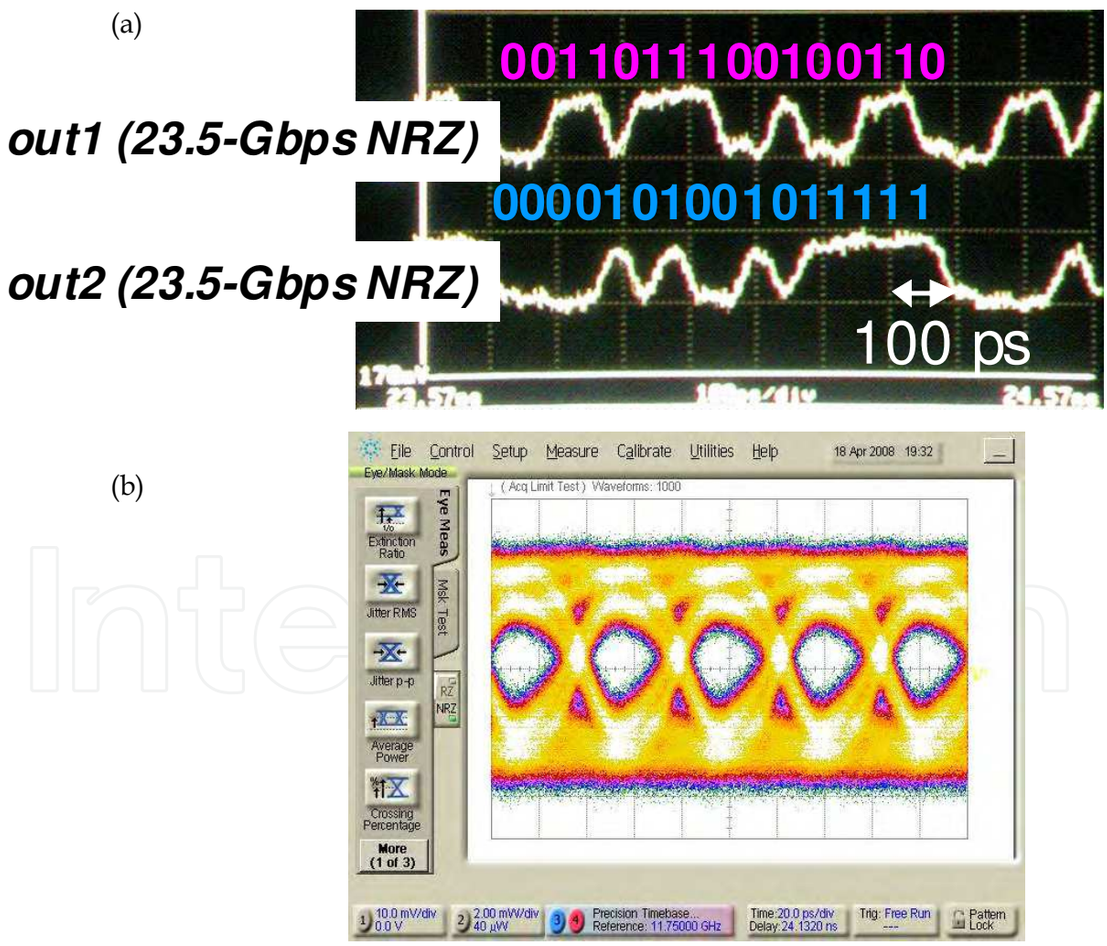

Fig. 18. Experimental results of optical input at data rate of 47 Gbps using SFQ test chip; (a) 23.5-Gbps digital output waveforms of two SQUID drivers and (b) eye pattern of one output for PRBS data input.

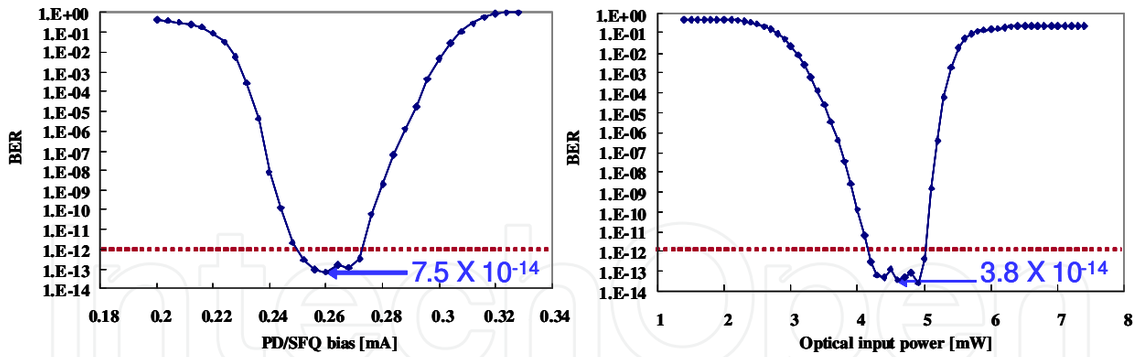

Fig. 19. Bit error rate (BER) as function of (a) bias current of PD-SFQ converter and (b) optical input power for UTC-PD module.

4.3 Josephson voltage standards

Josephson voltage standards (JVS) have been used as a DC voltage standard since 1990 because of their quantum mechanical accuracy. These standards consist of an under-damped superconductor-insulator-superconductor (SIS) junction array, which is DC biased and radiated with microwave. The voltage is determined with the microwave frequency and physical constant, which ensure its quantum mechanical accuracy. Although, JVS are suitable for DC voltage standards, they cannot be applicable to AC voltage standards. Because JVS use the hysteresis of SIS junctions, a proper procedure for applying the DC bias and microwaves and time to fix to the desired voltage is required.

The pulse-driven Josephson arbitrary waveform synthesizer (PD-JVS) is a device for producing AC voltage standard, which is one of AC JVS. This device is also called as Josephson arbitrary waveform synthesizer (JAWS). The principle is based on a 1-bit sigma delta digital-to-analog converter. The basic idea is that the amplitude of a signal waveform is represented as a pulse density. The pulse pattern is properly calculated for desired waveform and generated with a pulse pattern generator, which is applied to a JAWS chip. The JAWS chip consists of over-damped Josephson junction arrays (JJAs), which are capable of producing quantized voltage pulses. High-speed pulses, of which a pattern is calculated for producing the desired waveform, is generated in room-temperature electronics, and the optical signal is transferred to an electrical signal with the customized UTC-PD module at cryogenic temperature, which enables us to apply the high-speed signal to the SFQ chip with extremely low noise as well as low signal losses and distortions. The operation of the synthesizer was demonstrated by the National Institute of Advanced Industrial Science and Technology (AIST) and ISTEC using the cooling system with the customized UTC-PD module. We have to use junctions without hysteresis for the JAWS. The JAWS chips were fabricated in two superconducting microchip processes; one with Nb/AlOx/Al/AlOx/Nb Josephson junctions, which are superconductor-insulator-normal metal-superconductor (SINS) junctions, developed by ISTEC, and the other with NbN/TiNx/NbN junctions, which are superconductor-normal metal-superconductor (SNS) junctions, developed by AIST. Figure 20 shows an IC chip fabricated with the Nb/AlOx/Al/AlOx/Nb junctions.

The chip consists of an array of 100 serially connected junctions, which can increase the output voltage. The array was arranged in the center of a 50 Ω coplanar waveguide input line in the chip. The 5 x 5 mm chip was flip-chip bonded on the MCM carrier, in the same manner as SFQ chips. PD-JVS chips were also fabricated with the NbN/TiNx/NbN

junctions, in which 480 junctions were serially connected to increase the output voltage. The chip using the NbN junctions can operate at higher temperatures than that using the Nb junctions, which enable us to use a 10-K cryocooler.

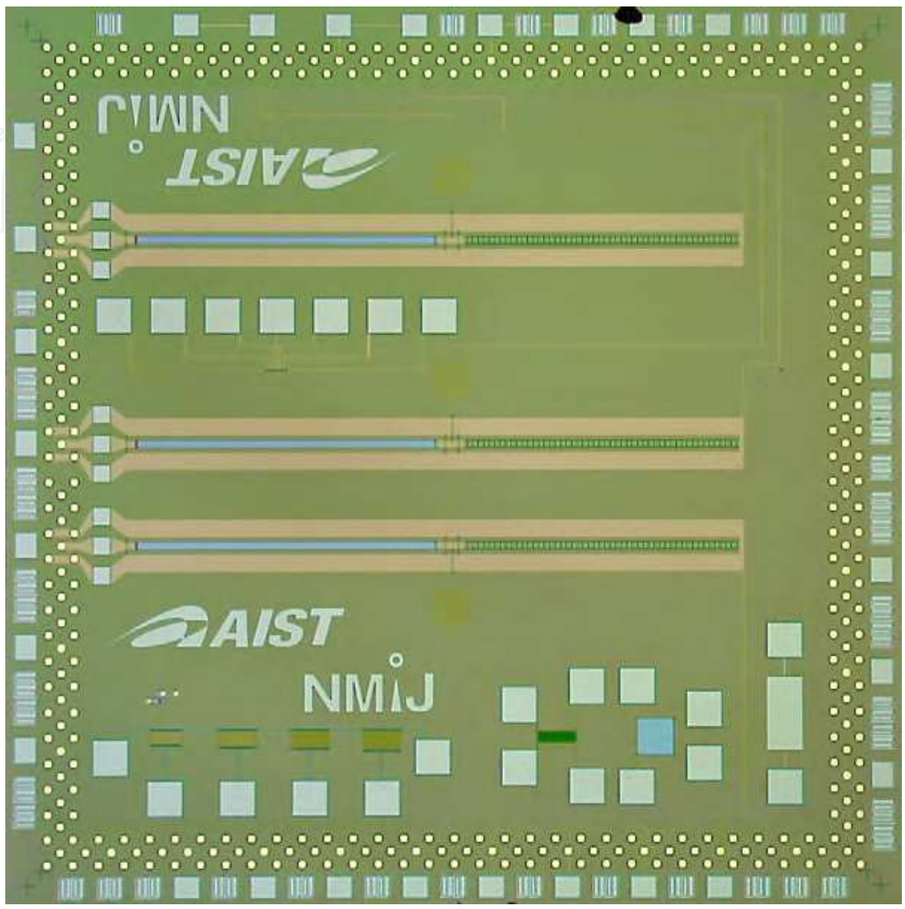

Fig. 20. Microphotograph of pulse-driven Josephson arbitrary waveform synthesizer (PD-JVS) chip fabricated with Nb/AlOx/Al/AlOx/Nb junction technology.

The JAWS can produce any waveform by applying a properly calculated pulse pattern. Figure 21 shows examples of synthesized waveforms; (a) triangular, (b) rectangular, and (c) saw-tooth. The left charts show the frequency spectrum and the right ones show generated waveforms. A high-precision sine wave was generated with a JAWS chips fabricated with both Nb/AlOx/Al/AlOx/Nb and NbN/TiNx/NbN Josephson junctions. Figure 22 shows the frequency spectrum of a 152.6-kHz sine wave with the PD-JVS using the Nb junctions. The sampling frequency was 10 GHz and the output voltage of 1.24 mV with spurious free dynamic range (SFDR) of -75 dBc was obtained from the chip. Figure 23 shows the frequency spectrum of a 59.6-Hz sine wave generated with the 480 NbN-SNS junctions, of which the frequency is important because it is around the commercial (mains) frequencies of 50 and 60 Hz. The sampling frequency was 8 GHz and a 134,217,728-bit-long (=2^{27} bit) binary pulse pattern was used for generating the 59.6-Hz sine wave. A sine wave was clearly observed with both PD-JVS chips. However, the SFDR was limited to -67 dBc due to odd harmonics of 50 Hz. The SFDR omitting these harmonics was as low as -80 dBc. The reduction of signal-to-noise

ratio (SNR) due to the odd harmonics of 50 Hz seemed to be affected by noise from the ground loops. The ground noise could be avoided by isolating the grounds in the I/Os.

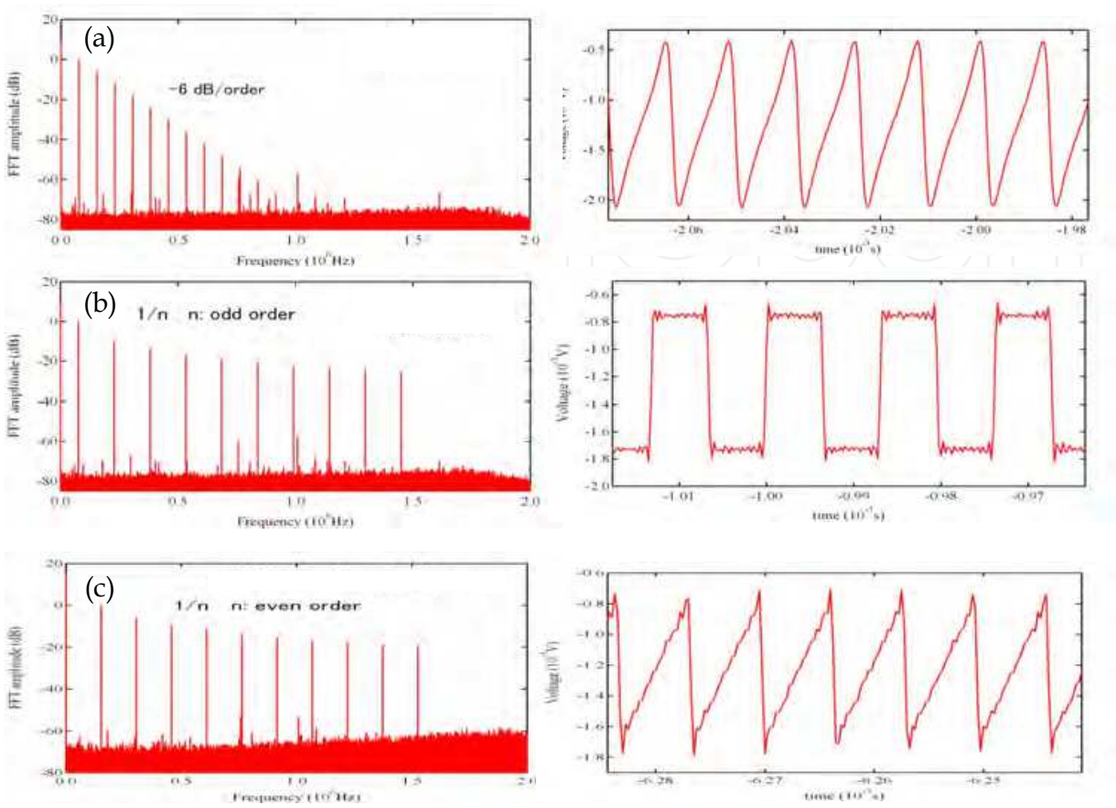

Fig. 21. Examples of frequency spectrum and waveforms synthesized using PD-JVS; (a) triangular, (b) rectangular, and (c) saw-tooth.

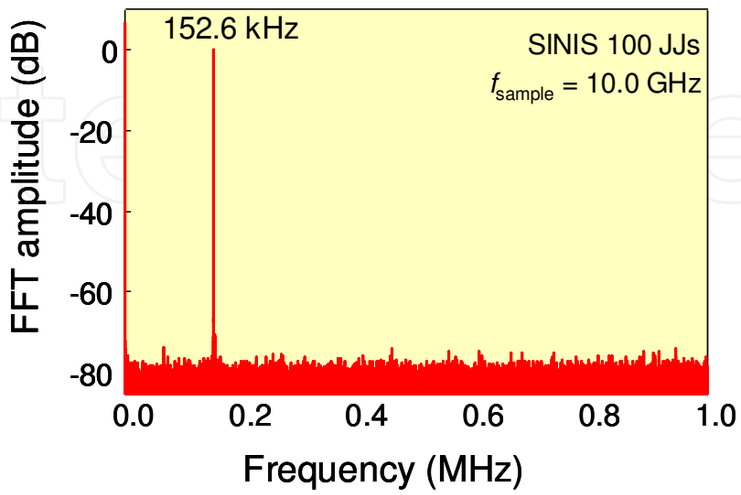

Fig. 22. Frequency spectrum of synthesized sine wave of 152.6 KHz with the PD-JVS using Nb/AlOx/Al/AlOx/Nb junctions.

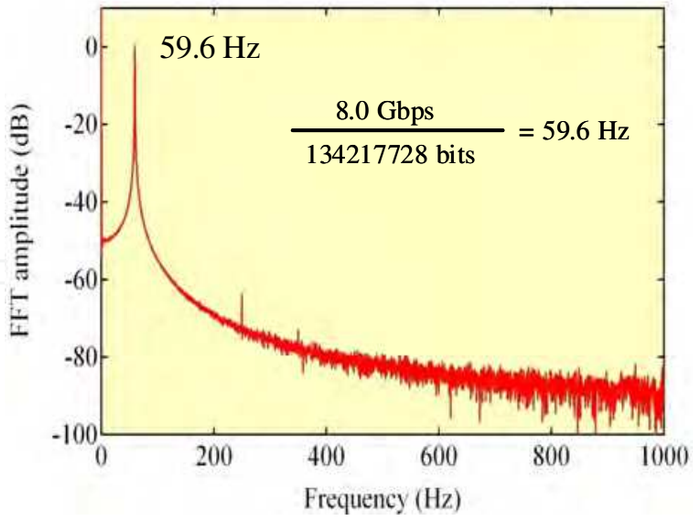

Fig. 23. Frequency spectrum of synthesized sine wave of 59.6 KHz with the PD-JVS using NbN/TiNx/NbN Josephson junctions

5. Conclusion

We studied the performance of a standard UTC-PD module at low temperature and developed a customized module for superconducting devices. In the customized module, an optical fiber lens was used to avoid using ferromagnetic material for fixing the optical lens. The performance of the customized UTC-PD modules at cryogenic temperature as low as 4 K was confirmed experimentally for the first time. High-speed operation of up to 40 Gbps was confirmed using a cryocooling system we developed for superconducting circuits, especially SFQ circuits. This cryocooling system uses a 4-K GM cryocooler and worked well for evaluating our customized UTC-PD module and for demonstrating superconducting circuits with high-speed data rate using an optical input link with our customized UTC-PD module and optical fibers. First, a basic SFQ digital circuit, which has a PD-SFQ converter with the output signal from the UTC-PD module for the input link, a 1-2 DEMUX, two sets of driver circuits for the output links, operated at a data rate of up to 47 GHz. Second, the performance of the PD-JVS with an optical input link was successfully demonstrated using the same cryocooling system at AIST in collaboration with ISTEC.

6. Acknowledgments

We would like to thank Tadao Ishibashi of NTT Electronics Ltd., and Takeshi Konno, Koichiro Uekusa, and Masayuki Kawabata of Advantest Lab. Ltd. for their contributions to the development of the UTC-PD for superconducting devices and their useful comments, and express our gratitude to Nobuhisa Kaneko, Chiharu Urano, Michitaka Maruyama for giving the result of a pulse-driven AC voltage standard. We also would like to thank Yoshiji Hashimoto for his many of contributions to this work, Michiyo Isaka and the members of ISTEC-SRL for fabricating the IC chips, and Mayumi Katsume for assembling the MCMs. We also express our gratitude to Seizo Akasaka of Kawashima Manufacturing Co, Ltd. for developing the MCM package and connector. The National Institute of Advanced Industrial Science and Technology partially contributed to the circuit fabrication. This work was partially supported by the New Energy and Industrial Technology Development

Organization (NEDO) as Development of Next-Generation High-Efficiency Network Device Project. The National Institute of Advanced Industrial Science and Technology (AIST) partially contributed to the circuit fabrication.

7. References

E.Zielinski, H.Schweizer, K.Streubel, H.Eisele, G.Weimann, *J. Appl. Phys.*, 59, no.6, pp.2196-2204(1986)

http://www.ioffe.ru/SVA/NSM//Semicond/GaInAs/optic.html

Goldberg Yu.A. and N.M. Schmidt *Handbook Series on Semiconductor Parameters*, vol.2, M. Levinshtein, S. Rumyantsev and M. Shur, ed., World Scientific, London, 1999, pp. 62-88

K. Likharev and V. K. Semenov, "RSFQ logic/memory family : A new Josephson-junction technology for sub-terahertz-clock frequency digital systems, " *IEEE Trans.Appl. Superconductivity*, vol. 1, no. 1, pp. 3–28, Mar. 1991

Y. Hshimoto, S. Yorozu, T. Satoh, and T. Miyazaki, "Demonstration of chip-to-chip transmission of single-flux-quantum pulses at throughputs beyond 100 Gbps, " Appl. Phys. Lett., 2005, 022502

Y. Hashimoto, S. Yorozu, T. Miyazaki, Y. Kameda, H. Suzuki, and N. Yoshikawa, "Implementation and experimental evaluation of a cryocooled system prototype for high-throughput SFQ digital applications," *IEEE Trans.Appl. Superconductivity*, vol. 17, no. 2, pp. 546–551, Jun. 2007

Y. Hashimoto, H. Suzuki, S. Nagasawa, M. Maruyama, K. Fujiwara, and M. Hidaka, "Measurement of superconductive voltage drivers up to 25 Gb/s/ch," *IEEE Trans.Appl. Superconductivity*, vol. 19, no. 3, pp. 1022–1025, Jun. 2009

M. Maruyama, K. Uekusa, T. Konno, N. Sato, M. Kawabata, T. Hato, H. Suzuki, and K. Tanabe, "HTS sampler with optical signal input," *IEEE Trans.Appl. Superconductivity*, vol. 17, no. 2, pp. 573–576, Jun. 2007

H. Ito, S. Kodama, Y. Muramoto, T. Furuta, T. Nagatsuma, and T. Ishibashi, "High-speed and High-output InP-InGaAs unitraveling-carrier photodiodes, " *IEEE J. Selected Topics in Quantum Electronics,* vol. 10, no. 4, pp. 709–727, July/Aug. 2004

H. Ito, T. Furuta, T. Nagatsuma, F. Nakajima, K. Yoshino, and T. Ishibashi, "Photonic generation of continuous THz wave using Uni-Traveling-carrier photodiode, " *IEEE J. Lightwave Technology,* vol. 23, no. 12, pp. 4016–4021, Dec. 2005

H. Suzuki, T. Hato, M. Maruyama, H. Wakana, K. Nakayama, Y. Ishimaru, O. Horibe, S. Adachi, A. Kamitani, K. Suzuki, Y. Oshikubo, Y. Tarutani, K. Tanabe, T. Konno, K. Uekusa, N. Sato, and H. Miyamoto, "Progress in HTS sampler development," Physica C 426-431, pp. 1643-1649, 2005

H. Suzuki, M. Maruyama, Y. Hashimoto, K. Fujiwara, and M. Hidaka, "Possible application of flash-type SFQ A/D converter to optical communication systems and their measuring instruments,", *IEEE Trans. Appl. Supercon.*. vol. 19, pp. 611-616, Jun. 2009

H. Suzuki, M. Oikawa, K. Nishii, K. Ishihara, K. Fujiwara, M. Maruyama, and M. Hidaka, "Design and demonstration of a 5-bit flash-type SFQ A/D converter integrated with error correction and interleaving circuits," to be published in *IEEE Trans. Appl. Supercon.*., Jun. 2011

T. Ishibashi, and N. Shimizu "Uni-traveling-carrier photodiode as an optoelectronic driver, " *OSA TOPS,* vol. 28, Ultrafast Electronics and Optoelectronics, John Bowers and Wayne Knox (eds.)

http://www.shf.de/fileadmin/download/Amp/Datasheet_SHF105C_V001.pdf

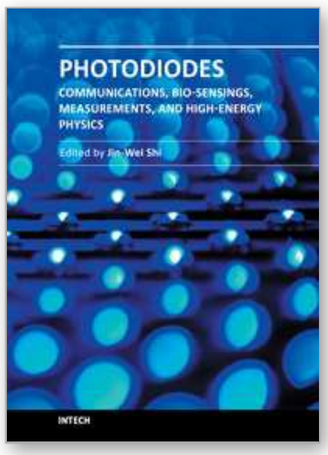

Photodiodes - Communications, Bio-Sensings, Measurements and High-Energy Physics

Edited by Associate Professor Jin-Wei Shi

ISBN 978-953-307-277-7
Hard cover, 284 pages
Publisher InTech
Published online 06, September, 2011
Published in print edition September, 2011

This book describes different kinds of photodiodes for applications in high-speed data communication, biomedical sensing, high-speed measurement, UV-light detection, and high energy physics. The photodiodes discussed are composed of several different semiconductor materials, such as InP, SiC, and Si, which cover an extremely wide optical wavelength regime ranging from infrared light to X-ray, making the suitable for diversified applications. Several interesting and unique topics were discussed including: the operation of high-speed photodiodes at low-temperature for super-conducting electronics, photodiodes for bio-medical imaging, single photon detection, photodiodes for the applications in nuclear physics, and for UV-light detection.

InTech Europe
University Campus STeP Ri
Slavka Krautzeka 83/A
51000 Rijeka, Croatia
Phone: +385 (51) 770 447
Fax: +385 (51) 686 166
www.intechopen.com

InTech China
Unit 405, Office Block, Hotel Equatorial Shanghai
No.65, Yan An Road (West), Shanghai, 200040, China
中国上海市延安西路65号上海国际贵都大饭店办公楼405单元
Phone: +86-21-62489820
Fax: +86-21-62489821

IntechOpen